A Dynamical Density Functional Study on the Reaction of Ethylene with $Cp_2Zr(C_2H_5)^+$

Peter Margl,[†] John C. W. Lohrenz,[†] Tom Ziegler,*[,†] and Peter E. Blöchl[‡]

Contribution from the Department of Chemistry, University of Calgary, 2500 University Drive N.W., T2N 1N4 Calgary, Alberta, Canada, and IBM Research Division, Zurich Research Laboratory, CH-8803 Rüschlikon, Zurich, Switzerland

Received October 19, 1995. Revised Manuscript Received February 21, 1996[⊗]

Abstract: Possible pathways for the reaction of ethylene with $Cp_2Zr(C_2H_5)^+$ are studied with the Car−Parrinello Projector Augmented Wave (CP-PAW) technique, which is based on density functional theory (DFT). "Slow growth" constrained first-principles molecular dynamics at 300 K were used to sample the phase space in the vicinity of the saddle points of the reactions. The simulations considered the growing chain in a resting state between insertions where a hydrogen on the β-carbon is attached to the metal. We have investigated three mechanisms, namely frontside (FS) insertion with ethylene approaching toward the β-agostic Zr−H bond, backside (BS) insertion with ethylene approaching toward the Zr−C_α bond, and hydrogen transfer (HT) chain termination with transfer of the β-agostic hydride to the incoming ethylene. Which pathway is followed is determined by the out-of-plane rotation of the ethyl group, which in turn is determined by the agostic interactions of the ethyl group. Agostic interactions are found to shift rapidly, with typical lifetimes of 0.5 ps for the FS insertion and 2 ps for the BS insertion. The activation barriers increase in the order front-side insertion < back-side insertion < hydrogen transfer. The shape of the potential surface obtained from previous static calculations was confirmed. The ethylene molecule is mobile enough to partake in fast exchange equilibria with surrounding substrate in solution.

1. Introduction

The interest in metallocene based olefin polymerization catalysts,[1] Scheme 1, has steadily grown in the last years and it is to be expected that metallocenes will eventually replace conventional Ziegler−Natta olefin catalysts based on titanium chlorides. This expectation has stimulated a number of theoretical investigations into the reaction mechanisms governing olefin polymerization catalyzed by metallocenes. Although the shape of the potential energy surface along the reaction path of Scheme 1 is fairly well studied by now,[2,3] only a single investigation[2p] has previously dealt with the dynamics of the different reaction pathways based on first-principles calculations. In the present study we attempt to elucidate the dynamics of the reaction between $Cp_2Zr(C_2H_5)^+$ and ethylene using the first-principles molecular dynamics method by Car[4] and Parrinello. Thus, in our study the growing chain of Scheme 1 is modeled by an ethyl group and the olefin by ethylene. Meier[2p] et al. have previously applied the Car−Parrinello method to the process in Scheme 1 with the growing chain modeled by a methyl group. However, a methyl group does not model the proper resting state in between insertion reactions and cannot be used to investigate some important chain termination reactions.[3a]

Elementary reaction steps in homogeneous catalysis have been investigated with increasing success by conventional electronic structure methods over the past decade.[5] Studies of this kind can provide minimum energy paths on the potential energy surface connecting reactant(s), transition state(s), and product(s). The conventional electronic structure methods afford essentially a static view of chemical reactions, although dynamical aspects and temperature effects can be included by statistical methods after mapping out the potential energy surface near the minimum energy paths. However, such a mapping is costly in terms of man hours and computer resources.

Car[4] and Parrinello (CP) have proposed a DFT based scheme in which the dynamics of a system can be studied from first principles without recourse to precalculated and fitted potential surfaces. Unfortunately, it is only practical to explore the

[†] University of Calgary.
[‡] Zurich Research Laboratory.
[⊗] Abstract published in *Advance ACS Abstracts,* April 1, 1996.

(1) Brintzinger, H. H.; Fischer, D.; Mülhaupt, R.; Rieger, B.; Waymouth, R. M. *Angew. Chem., Int. Ed. Engl.* **1995**, *34*, 1143.

(2) (a) Castonguay, L. A.; Rappé, A. K. *J. Am. Chem. Soc.* **1992**, *114*, 5832. (b) Armstrong, D. R.; Perkins, P. G.; Stewart, J. J. P. *J. Chem. Soc., Dalton Trans.* **1972**, 1972. (c) Cassoux, P.; Crasnier, F.; Labarre, J.-F. *J. Organomet. Chem.* **1979**, *165*, 303. (d) McKinney, R. J. *J. Chem. Soc., Chem. Commun.* **1980**, 490. (e) Balazs, A. C.; Johnson, K. H. *J. Chem. Phys.* **1982**, *77*, 3148. (f) Shiga, A.; Kawamura, H.; Ebara, T.; Sasaki, T.; Kikuzono, Y. *J. Organomet. Chem.* **1989**, *366*, 95. (g) Prosenc, M.-H.; Janiak, C.; Brintzinger, H.-H. *Organometallics* **1992**, *11*, 4036. (h) Kawamura-Kuribayashi, H.; Koga, N.; Morokuma, K. *J. Am. Chem. Soc.* **1992**, *114*, 8687. (i) Kawamura-Kuribayashi, H.; Koga, N.; Morokuma, K. *J. Am. Chem. Soc.* **1992**, *114*, 2359. (j) Fujimoto, H.; Yamasaki, T.; Mizutani, H.; Koga, N. *J. Am. Chem. Soc.* **1985**, *107*, 6157. (k) Novaro, O.; Blaisten-Barojas, E.; Clementi, E.; Giunchi, G.; Ruiz-Vizcaya, M. E. *J. Chem. Phys.* **1978**, *68*, 2337. (l) Weiss, H.; Ehrig, M.; Ahlrichs, R. *J. Am. Chem. Soc.* **1994**, *116*, 4919. (m) Siegbahn, P. E. M. *Chem. Phys. Lett.* **1993**, *205*, 290. (n) Sakai, S. *J. Phys. Chem.* **1991**, *95*, 7089. (o) Novaro, O. *Int. J. Quantum Chem.* **1992**, *42*, 1047. (p) Meier, R. J.; van Dormaele, G. H. J.; Iarlori, S.; Buda, F. *J. Am. Chem. Soc.* **1994**, *116*, 7274. (q) Bierwagen, E. P.; Bercaw, J. E.; Goddard, W. A., III *J. Am. Chem. Soc.* **1994**, *116*, 1481. (r) Jolly, C. A.; Marynick, D. S. *J. Am. Chem. Soc.* **1989**, *111*, 7968. (s) Axe, F. U.; Coffin, J. M. *J. Phys. Chem.* **1994**, *98*, 2567. (t) Fink, G. In *Recent Advances in Mechanistic and Synthetic Aspects of Polymerisations*; Fontanille, M., Guyot, A., Eds.; D. Reidel, Publishing: Dordrecht, The Netherlands, 1987; p 515.

(3) (a) Lohrenz, J. C. W.; Woo, T. K.; Fan, L.; Ziegler, T. *J. Am. Chem. Soc.* **1995**, *117*, 12793. (b) Fan, L.; Harrison, D.; Woo, T. K.; Ziegler, T. *Organometallics* **1994**, *1995*, *14*, 2018. (c) Woo, T. K.; Fan, L.; Ziegler, T. In *40 Year Ziegler-Catalyses*; Freiburg/Breisgau, Germany, 1993; in press. (d) Woo, T. K.; Fan, L.; Ziegler, T. *Organometallics* **1994**, *13*, 2252. (e) Woo, T. K.; Fan, L.; Ziegler, T. *Organometallics* **1994**, *13*, 423. (f) Fan, L.; Harrison, D.; Deng, L.; Woo, T. K.; Swerhone, D.; Ziegler, T. *Can. J. Chem.* **1995**, *73*, 989. (g) Lohrenz, J. C. W.; Woo, T. K.; Fan, L.; Ziegler, T. *J. Organomet. Chem.* **1995**, *497*, 91.

(4) Car, R.; Parrinello, M. *Phys. Rev. Lett.* **1985**, *55*, 2471.

(5) (a) *Theoretical Aspects of Homogeneous Catalysis*; van Leeuwen, P. W. N. M., Morokuma, K., van Lenthe, J. H., Eds.; Kluwer Academic Publishers: Dordrecht, The Netherlands, 1995;

S0002-7863(95)03510-4 CCC: $12.00

Scheme 1. Olefin Polymerization by Metallocene

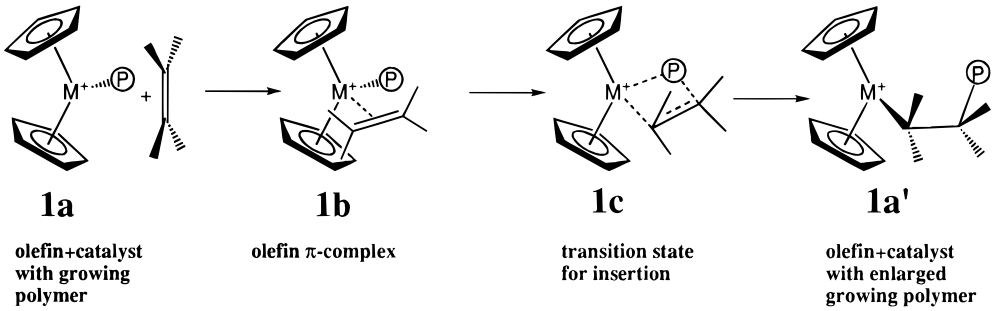

regions of phase space relevant for chemical reactions with straightforward dynamics if low barriers are involved. For processes with high or even moderate barriers (>30 kJ/mol), the events of interest occur sparsely, if at all. Most of the simulation time is thus spent in the more trivial places in phase space, rendering the simulation computationally costly and inefficient.

In the present study we employ a technique based on constrained CP dynamics, where we introduce fictitious dynamics along a chosen reaction coordinate in order to sample the phase space in the vicinity of the transition state (TS). The appropriate reaction coordinate as well as the area around the transition state has already been mapped by conventional[3a] electronic structure calculations based on the Amsterdam Density Functional program system[6] (ADF). The CP dynamics is carried out with the projector augmented wave method (PAW) due to Blöchl.[7]

2. Computational Details and Methodology

All reported molecular dynamics simulations were carried out with the Car−Parrinello Projector Augmented Wave (CP-PAW) code developed by Blöchl.[7] The wave function is expanded in plane waves up to an energy cutoff of 30 Ry. The frozen-core approximation was applied for shells below the 4d electrons of Zr and for the 1s electrons of C. Core data were imported from scalar relativistic atomic calculations. All simulations were performed using the local density approximation in the parametrization of Perdew and Zunger,[8] with gradient corrections due to Becke[9] and Perdew.[10] This enables us to directly compare structures and energetics with ref 3a, which used equivalent functionals. We use periodic boundary conditions with a 11.3 Å fcc cell, which was found to be sufficiently large to prevent wave function overlaps between neighboring images. Long-range electrostatic interactions between different cells are eliminated using a method developed by Blöchl.[11] A time step of 10 au is used to integrate the equations of motion, correcting the mass of the nuclei to account for the drag of the electrons[12] in the coupled dynamics integrated with the Verlet[13] algorithm. The temperature of the nuclei is controlled by a Nosé[14] thermostat, which creates a canonical (NVT) ensemble. To achieve an evenly distributed thermal excitation, all systems were equilibrated for 30 ps with classical molecular dynamics with the MacroModel program, using a force field fitted to the results of nonlocal ADF calculations.[15]

To sample phase space in the vicinity of the transition state, we choose a reaction coordinate (RC) which is kept constrained during the dynamics using SHAKE[16] constraints. It is desirable that the RC has a high projection onto the IRC[17] (intrinsic reaction coordinate). All other degrees of freedom are allowed to evolve naturally in time. By slowly varying the constraint, phase space in the vicinity of the transition state can be sampled dynamically,[18] leading to undisturbed dynamics for all motions which are orthogonal to the RC, and to fictitious dynamics along the RC. This allows us to investigate even high-lying transition states. The speed of the RC scan was determined by a third-power polynomial, to avoid sudden accelerations which disrupt the coupled electron-ion dynamics. The total scan time chosen was about 20 000 time steps (=4.8 ps) for all simulations.

The free energy difference ΔF between two arbitrary points $\lambda = 0$ and 1 along the reaction coordinate can be determined as

$$\Delta F = \int_0^1 \langle \partial E/\partial\lambda \rangle|_{\lambda,T}\, \mathrm{d}\lambda \qquad (1)$$

where λ is just a linear parameter representing any path connecting the two points and the integrand is the appropriately scaled averaged force on the RC sampled at constant temperature and λ.[19] For eq 1 to give correct results, $\langle \delta E/\delta\lambda \rangle$ must be determined at a large number of λ-points between 0 and 1. Furthermore, for each λ-point an extensive sampling is required at constant T to determine the proper average $\langle \delta E/\delta\lambda \rangle_{\lambda,T}$. In the "slow growth" limit, λ is scanned continuously so that only a single value of $\delta E/\delta\lambda$ is determined at each value of λ. This method[18] has the advantage of not disrupting the dynamics when the value of λ is changed. However, since systematic errors are introduced by the finite scan speed, λ has firstly to be scanned very slowly and secondly a hysteresis curve has to be sampled to remove systematic errors from the simulation. Preliminary tests have shown that in order to obtain accurate values for ΔF, the simulation time (currently ≈5 ps) for a scan in one direction must probably be increased by a factor of 5. We therefore will give tentative values for $\Delta F^{\ddagger}$ and ΔF based on a unidirectional scan along the RC. These tentative values will be designated $\Delta F_N^{\ddagger}$ and ΔF_N to indicate their nonequilibrium character.

We can further use the integral $I(\lambda) = \int \langle \delta E/\delta\lambda \rangle_{\lambda,T}\, \mathrm{d}\lambda$ to identify stationary points along RC by observing that $I(\lambda)$ has a minimum at equilibrium geometries and a maximum at transition states. Throughout the following sections, we use the following nomenclature to designate stationary points on the potential surface: The reaction pathway along which the stationary point is found will be described by a prefix, i.e. FS, BS, or HT for front-side insertion, back-side insertion, and hydrogen transfer reaction, respectively. Furthermore, a suffix will be used to indicate *where* on the RC a specific stationary point is found: −S (**s**tarting structure) indicates the precursor complex, −TS indicates the **t**ransition **s**tate, and −E (**e**nd structure) designates the product of the

(6) ADF version 1.1.3.
(7) Blöchl, P. E. *Phys. Rev. B* **1994**, *50*, 17953.
(8) Perdew, J. P.; Zunger, A. *Phys. Rev. B* **1981**, *23*, 5048.
(9) Becke, A. D. *Phys. Rev.* **1988**, *A38*, 3098.
(10) Perdew, J. P. *Phys. Rev. B* **1986**, *33*, 8822; **1986**, *34*, 7406.
(11) Blöchl, P. E. *J. Chem. Phys.* **1995**, *103*, 7422.
(12) Blöchl, P. E.; Parrinello, M. *Phys. Rev. B* **1992**, *45*, 9413.
(13) Verlet, L. *Phys. Rev.* **1967**, *159*, 98.
(14) (a) Nosé, S. *Mol. Phys.* **1984**, *52*, 255. (b) Hoover, W. G. *Phys. Rev. A* **1985**, *31*, 1695.
(15) Lohrenz, J. C. W.; Ziegler, T. presented at the 209th ACS National Meeting, Anaheim, CA, April 2−6, 1995.
(16) Ryckaert, J.-P.; Ciccotti, G.; Berendsen, H. J. *J. Comp. Phys.* **1977**, *23*, 327.
(17) Fukui, K. *Acc. Chem. Res.* **1981**, *14*, 363.
(18) (a) Straatsma, T. P.; Berendsen, H. J. C.; Postma, J. P. M. *J. Chem. Phys.* **1986**, *85*, 6720. (b) Singh, U. C.; Brown, F. K.; Bash, P. A.; Kollman, P. A. *J. Am. Chem. Soc.* **1987**, *109*, 1607.
(19) Milman, V.; Payne, M. C.; Heine, V.; Needs, R. J.; Lin, J. S.; Lee, M. H. *Phys. Rev. Lett.* **1993**, *70*, 2928.
(20) (a) Burger, B. J.; Thompson, M. E.; Cotter, W. D.; Bercaw, J. E. *J. Am. Chem. Soc.* **1990**, *112*, 1566. (b) Thompson, M. E.; Buxter, S. M.; Bulls, A. R.; Burger, B. J.; Nolan, M. C.; Santarsiero, B. D.; Schaefer, W. P.; Bercaw, J. E. *J. Am. Chem. Soc.* **1987**, *109*, 203.

reaction. The latter were detected by minima in $I(\lambda)$, transition states by the respective maxima. Precursor structures were taken from ref 3a since the respective minima in $I(\lambda)$ were too flat to localize them reliably. This approximation is validated by the close agreement observed between both our results and those of ref 3a for transition states and product structures (section 3). Note that suffixes (-S, -E) refer to the locations of stationary points on the path and do not indicate where the simulation was actually started and terminated, respectively.

Our treatment of atomic nuclei is purely classical and therefore cannot account for effects which are contributed by the quantum mechanical behavior of the atomic nuclei, such as the zero-point vibrational energy. Since in the present system the barrier heights are in the order of magnitude of the zero-point energies, care must be taken in comparing our results to experiment or other theoretical results which might account for these phenomena.

3. Results and Discussion

One of the recurring problems encountered in modeling of the insertion process is associated with a lack of structural information about the active species **1a** of Scheme 1. Thus, little is known about the coordination geometry of the growing chain attached to the L_2M fragment in its resting state between insertions. Calculations[2i,2l,3] on L_2MR^+ systems in which R is propyl have revealed that the most stable structure has a β-agostic conformation, **2a**, in which a single $C_\beta-H$ bond is directed toward the metal center. Of somewhat higher energy is the γ-agostic species, **2b**. In this investigation, we regard the structure **2a** as a possible resting state for **1a** with R′ representing the growing chain. A β-agostic conformation has been established by Bercaw[20] et al. for $Cp^*_2Sc(Et)$.

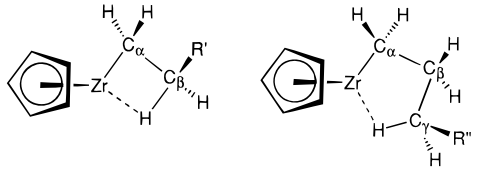

2a **2b**

With **2a** as a model for the resting state of **1a**, one might envision two insertion paths for an approaching olefin. The first, **3a**, involves an approach of olefin toward the Zr−H agostic bond. It will be referred to as the front-side (FS) attack. The second, **3b**, has olefin attacking the $Zr-C_\alpha$ bond, and will be referred to as the back-side (BS) attack. We shall investigate both paths in detail with R′ of **2a** modeled by hydrogen. Lohrenz et al.[3a] have already shown from static DFT calculations that the ethylene molecule forms stable π-complexes (**1b**) with $Cp_2Zr(C_2H_5)^+$ which act as precursors for the actual insertion processes **3a** and **3b**.

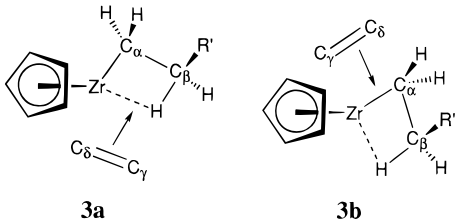

3a **3b**

The growth of the polymer will eventually be stopped by chain termination. Experimental work[1] as well as theoretical calculations[3a,b,d,f,g] indicate that one of the more likely chain terminating mechanisms involves the hydrogen-exchange reaction, **4**. In this process, olefin approaches the metal center from its front-side and forms a π-complex. In the transition state the β-hydrogen is transferred to the olefin and a vinyl-terminated polymer chain is eliminated. The newly formed alkyl−metallocene then can start a new chain. We shall include the hydrogen-exchange reaction **4** in our molecular dynamics study.

Scheme 2

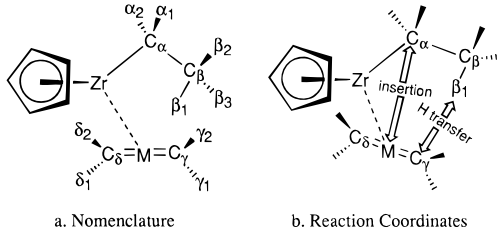

a. Nomenclature b. Reaction Coordinates

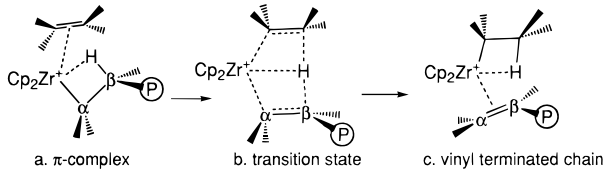

a. π-complex b. transition state c. vinyl terminated chain

4

a. Simulation of the Front-Side Attack without Constraints (FS-BS). For our CP-PAW simulation of the front-side approach, **3a**, we chose the distance between the α-carbon atom of the ethyl group (C_α) and the center-of-mass of the ethylene carbon atoms (M) as our reaction coordinate (RC) (Scheme 2). Previous calculations[3a] with density functionals equivalent to ours have shown that the equilibrium $C_\alpha-M$ distance of the front-side olefin π-complex **1b** is 4.27 Å. We initialize the simulation at a point in phase space where the $C_\alpha-M$ distance is 4.5 Å (Table 1), in order to "capture" the behavior of the ethylene before the actual π-complex is formed. The reaction coordinate length (RCL) was slowly decreased over the next 4.8 ps (=20 000 time steps). We did not apply any constraints other than the RC in this simulation. As we now shall show, this unconstrained simulation leads to a rotation of the ethyl group around the $M-C_\alpha$ axis resulting in a precursor state for the back-side insertion reaction **3b**. Therefore we will refer to this simulation as the FS-BS simulation. We performed a total of two simulations of this kind, which were started from different points in phase space. Since they yielded almost identical results, only one of them is presented here.

Structure. In Figure 1, we show selected snapshots from the simulation, whereas important structural and energetic quantities of the reactants are monitored as a function of RCL in Figure 2. Although the reaction $Cp_2Zr(C_2H_5)^+ + C_2H_4 \rightarrow [Cp_2Zr(C_2H_5)(C_2H_4)]^+$ is exothermic by −37 and −44 kJ/mol, respectively, for the front-side and the back-side pathways according to ref 3a, the ethylene moiety is quite mobile throughout the reaction. Figures 1A−C show that it rotates freely about the Zr−M axis. It also undergoes large-amplitude wagging motions out of the plane which separates the two Cp rings. The extent of this rotation is visible in Figure 2B (angle $C_\gamma-M-Zr-C_\alpha$). Its amplitude diminishes at smaller values of the RCL, since the incipient formation of the $C_\gamma-C_\alpha$ bond (at RCL ≈ 2.5 Å) fixes its spatial orientation. This confirms results from a previously conducted CP-PAW simulation without RC constraint,[21] which show that the ethylene moiety is quite capable of dissociating from the metal center at 300 K.[22] Before

(21) Margl, P.; Lohrenz, J. C. W.; Ziegler, T.; Blöchl, P. E. Unpublished result.

(22) The average kinetic energy of the ethylene moiety at 300 K can be calculated to be 22.4 kJ/mol according to the equipartition theorem, compared to a dissociation energy of 37 kJ/mol for the FS π-complex. Since the instantaneous kinetic energy can be much higher, dissociation is quite facile.

Table 1. Parameters for Molecular Dynamics Simulations of the Front-Side Insertion, Back-Side Insertion, and Hydrogen Transfer Reaction[a]

		RCL						
simulation	reaction coord	start[b,c]	end[b,c]	RCL_S[b,d]	RCL_{TS}[b,e]	RCL_E[b,f]	$\Delta F_N^{\ddagger}$ (S → TS)[g]	ΔF_N (S → E)[g]
front-side insertion	M−C_α	4.27	1.85		2.76	2.15	20 ± 10	−30 ± 10
				[4.271][h]	[2.769][h]	[2.153][h]	[8.55][h]	[−34.2][h]
back-side insertion	M−C_α	3.15	1.85		2.51	2.11	21 ± 10	−28 ± 10
				[2.974][h]	[2.520][h]	[2.106][h]	[33.2][h]	[−25.9][h]
hydrogen transfer	C_γ−β(1)	2.50	1.1		1.51	1.16	35	0
				[1.87][h]	[1.422][h]	[1.179][h]	[29.6][h]	[0.0][h]

[a] $\Delta F_N^{\ddagger}$ values are compared with $\Delta G^{\ddagger}$ values of Lohrenz et al., calculated according to $\Delta G^{\ddagger} = \Delta H_{elec}^{\ddagger} - 300 \cdot \Delta S_{tot}^{\ddagger}$ from Table 1 in ref 3a. ΔF_N values are compared to ΔH values from ref 3a. Values for FS insertion are derived from the simulation with rotational constraint (section 3b). No ΔF_N values are given for the front-side−back-side simulations since nonequilibration effects led to meaningless results. No vibrational quantum corrections are added to PAW energies. No vibrational quantum corrections are included in energies taken from ref 3a. [b] In units of angstrøm. [c] Length of the RC at the beginning/end of the simulation. [d] Length of the RC for the stable precursor complex. Values were inferred from ref 3a (see text). [e] Length of the RC for the transition state. [f] Length of the RC for the product. [g] In units of kJ/mol. [h] Value taken from ref 3a.

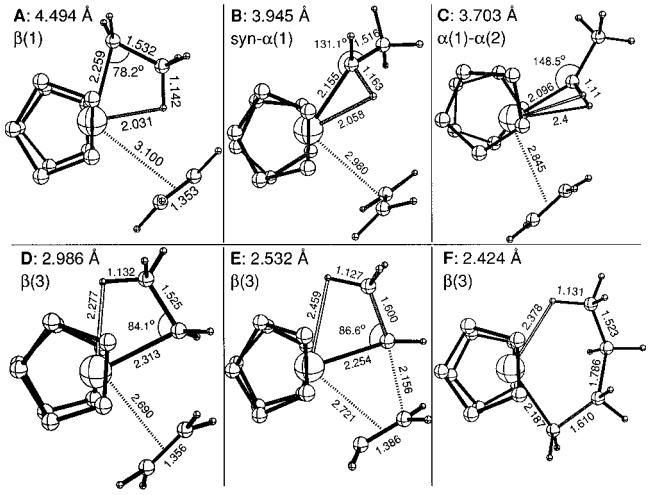

Figure 1. Selected snapshots from the FS-BS reaction simulation, sequentially numbered from A to F. Numbers in the upper left corners of the snapshots refer to the RCL at which the snapshot was taken, together with the hydrogen atom with the dominant agostic interaction. Bond distances in angstrom units and angles in degrees.

formation of the interaction between C_γ and C_α (RC > 3 Å), the Zr−M distance oscillates between 2.5 and 3.5 Å (Figures 1A−C). We conclude from these data that in solution the complexed ethylene molecule will probably partake in rapid exchange equilibria with the surrounding solvent.

We find the agostic interactions of the ethyl group (Figure 2A) to be highly correlated with the torsion angle M−Zr−C_α−C_β and the angle Zr−C_α−C_β (Figure 2B). The agostic interactions are more stable in the eventually formed back-side β-agostic insertion precursor (Figure 2A; 3−2 Å RCL) than in the initial front-side insertion precursor (Figure 2A; 4.5−3.5 Å RCL). Due to the steric pressure which is exerted by the approaching olefin, the β-agostic interaction of the terminal methyl group with Zr is weakened considerably as long as the ethyl group points toward the ethylene molecule. Due to this high mobility, agostic interactions in the front-side precursor shift rapidly, with a characteristic lifetime in the order of 0.5 ps. Switching between agostic interactions occurs on a time scale of about 0.1 ps, in accordance with the oscillation periods of typical skeletal frequencies which mediate the change. The first agostic interaction formed (β_1) remains intact for about 0.5 ps (Figure 2A), to be replaced by another agostic interaction of the same type (β_2), by rotation of the terminal methyl group. At RCL = 4 Å, a rotation of the ethyl group around the C_α−Zr axis and a widening of the Zr−C_α−C_β angle (Figure 2B) causes the β_2 interaction to break, and to be replaced by an *syn* α-agostic interaction (α_1, Figure 1B) at RCL = 3.8 Å. This

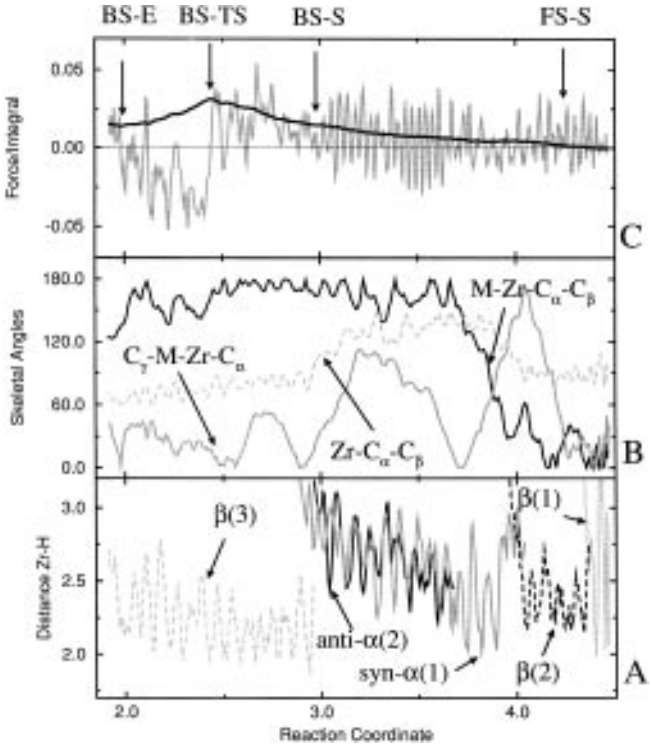

Figure 2. Structural and energetic quantities of the FS-BS insertion simulation as a function of RCL. (A) Agostic bond distances between Zr and various hydrogen atoms. For the sake of clarity only the dominant interaction at a time is shown. (B) Skeletal angles of the C_2H_4−Zr−C_2H_5 moiety. (C) Force on the RC (shaded line) and its integral (full line, see text). Arrows indicate the locations of the FS insertion precursor structure (FS-S; =FS resting state determined by ADF[3a]), the BS insertion precursor structure (BS-S; =BS resting state determined by ADF[3a]), the BS insertion transition state (BS-TS), and the BS insertion δ-agostic resting state (BS-E). The locations of BS-TS and BS-E were determined from the maximum and minimum, respectively, of the integral over the force on the RC. Suffixes -S and -E refer to start and end of the reaction channel, respectively. Distances in angstrom units, angles in degrees, and force on the RC and its integral in atomic units.

widening of the Zr−C_α−C_β angle upon rotation of the ethyl out of the molecular plane has also been observed by Lohrenz et al.[3a] Between 3.7 and 3 Å RCL, the α-agostic interactions are very flexible and extremely weak. Instead of forming a strong single agostic bond, both of the α-hydrogen atoms form a loose interaction with Zr (Figure 1C). We note that the favorable *anti* α-agostic interaction found by Lohrenz et al.[3a] is only rudimentarily formed in this simulation (below RCL = 3.6 Å). The reason for this is that the rotation of the ethyl group proceeds too fast to allow this interaction to be formed. As

rotation around the $C_\alpha-Zr$ axis is completed and the $Zr-C_\alpha-C_\beta$ angle closes to form the precursor for back-side attack (R = 3 Å), the β-agostic interaction is restored (Figures 1D and 2A). The ethyl group is held in place rigidly throughout the following back-side insertion reaction by this very stable β-agostic interaction.

Given that our simulation involves no steric barrier to ethyl rotation other than the one presented by the Cp hydrogen atoms, it is understandable that a reaction pathway is chosen which involves creating the starting complex for BS insertion, which is stabilized[3a] over the starting complex for FS insertion by about 7 kJ/mol. It should be noted that this FS-BS attack involves inversion of the metal center.

Energetics. Figure 2C shows the force on the RC ($\delta E/\delta\lambda$; shaded line) and the integral $\Delta F_N^{0\rightarrow RC} = \int_0^{RC} (\partial E/\partial\lambda)\, d\lambda$, where $\lambda = 0$ corresponds to the start of the simulation.[23] Since the reaction starts out in the FS channel and is pushed over into the BS channel, we marked the starting (−S), transition state (−TS), and end (−E) structures of the different pathways with arrows (values for starting structures taken from ref 3a). The TS and end point were marked where the integral curve had a maximum and minimum, respectively. Starting points were inferred from ADF calculations.[3a] The force on the RC rises slowly, and the transition state (zero of force) for back-side insertion is reached at RCL = 2.43 Å. The δ-agostic product state is reached at 2.01 Å RCL.

b. Simulation of the Front-Side (FS) Insertion with Rotational Constraint. The FS-BS simulation presented in Section 3a showed that without steric blockage of the back-side insertion path, the system chose the BS insertion path rather than the FS insertion path, even when the simulation was started from the precursor complex of front-side insertion. This crossing of reaction channels not only prevented a quantitative evaluation of the force on the RC, but also hindered further analysis of the specific reaction channels.

To force the system to undergo front-side insertion, we blocked the pathway to back-side insertion by introducing an external potential for the torsion angle $C_\delta-Zr-C_\alpha-C_\beta$, which serves to mimic the steric influence of a restraining group. The potential is constructed to be zero if the angle is smaller than 100°, and is parabolically increasing with a spring constant of 2 kJ/(mol deg^{-2}) beyond that. Introducing a hard-wall-like potential as described is equivalent to blocking the channel in phase space which interconnects the front-side and back-side insertion pathways.[24] The initialization procedure of the simulation was identical to the one applied in Section 3a. The reaction coordinate ($M-C_\alpha$) was scanned from 4.27 to 1.85 Å over 20 000 time steps (Table 1).

Structure. Restraining the torsion angle $C_\delta-Zr-C_\alpha-C_\beta$ has no notable effect on the agostic interactions, which show a behavior very similar to the FS-BS simulation without the confinement potential. Figure 4A shows that the dominant agostic interaction at the onset of the simulation is mediated by H(β_1) (Figure 3A). As in Section 3a, this β-agostic interaction is soon replaced by an α_2-agostic (*syn*) one (Figure 3B) at RCL ≈ 4 Å. The short lifetime of the β-agostic bond is due to the steric "pressure" which is exerted by the approaching ethylene and which forces the ethyl group to move out of the molecular midplane. This is accompanied by growth of the $Zr-C_\alpha-C_\beta$ angle (Figure 3B/4B) to about 130°. In accord with the switching of agostic interactions, the $M-Zr-C_\alpha-C_\beta$ torsion angle rises at the same time (Figures 3B/4B). The effect of the external potential is to keep the system from falling into the back-side channel, therefore the latter angle stays in the region between 110° and 60° most of the time. As expected (see Section 3a), the ethylene molecule is very mobile (Figure 3A−D). Due to its high mobility the ethylene hydrogens form extremely short lived (lifetime <0.05 ps) intermediate agostic interactions with the Zr center (see Figure 3C) by simultaneous rotations about the C═C and Zr−M axes. In *vitro*, this could be a source of Zr-mediated C−H activation. The orientation of the ethylene molecule is stabilized by contact between C_α and C_γ (around 3 Å RCL, Figure 4B). As in the FS-BS case, the change between *syn* and *anti* α-agostic bonds, which leads to the transition state for FS insertion (Figure 3E), proceeds slowly over a longer period of the reaction scan (RCL = 3.7−3.3 Å, Figure 3C/4A) where no appreciable agostic bonding exists. At RCL = 3.3 Å, the *anti* α_1-agostic bond is formed which anchors the transition state geometry. The agostic bond via H(α_1) remains stable until the end of the reaction (Figure 4A). As the reaction reaches the transition state (2.76 Å RCL, Table 1, Figure 4C), the potential superimposed on the torsion angle $C_\delta-Zr-C_\alpha-C_\beta$ becomes redundant, since the ethyl group is now spatially removed from the metal center and forms part of the alkyl chain. The external potential was therefore removed at RCL = 2.3 Å.

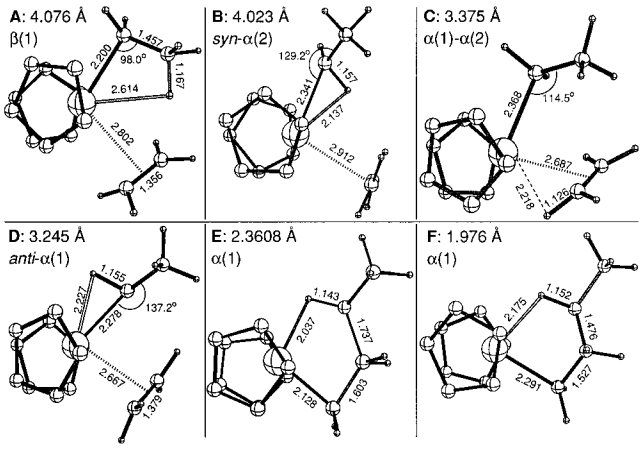

Figure 3. Selected snapshots from the FS reaction simulation, sequentially numbered from A to F. For legends and units see also Figure 1.

However, we did not find evidence of further stationary points on the potential surface except the FS precursor (which remains stable from 4.27 to 4.0 Å RCL), the FS transition state, and the γ-agostic FS insertion product. We therefore reason that the β-agostic conformation is indeed the true precursor for the front-side insertion path.

Energetics. The slow growth method yields free energy differences between species lying on the reaction path. However, prior experience states that for accurate estimates of ΔF for systems comparable to ours, the total simulation time has to be extended by a factor of at least 5, including sampling of hysteresis behavior. Therefore we confine ourselves to a more qualitative interpretation of the force on the constraint and its integral. In Figure 4C, arrows indicate the locations of the FS precursor resting state (right), the FS-insertion transition state (middle) and the γ-agostic product state (left) along the RC axis, as determined from the extremum points of the force integral (transition state and product) and ADF calculations[3a] (precursor).

(23) Since in this simulation multiple reaction channels are scanned, this particular simulation is highly nonequilibrated. Therefore we refrain from discussing free energy differences along the RC.

(24) In the context of our simulation, its only effect upon the dynamics is to mimic stochastic collisions which force the ethyl group back into the plane which separates the Cp rings. This is not detrimental to the results of the simulation as long as the torsion angle does not make continuous contact with the "wall". In our simulation, the torsion angle connected only about 5 times with the external potential, each contact lasting less than 0.02 ps.

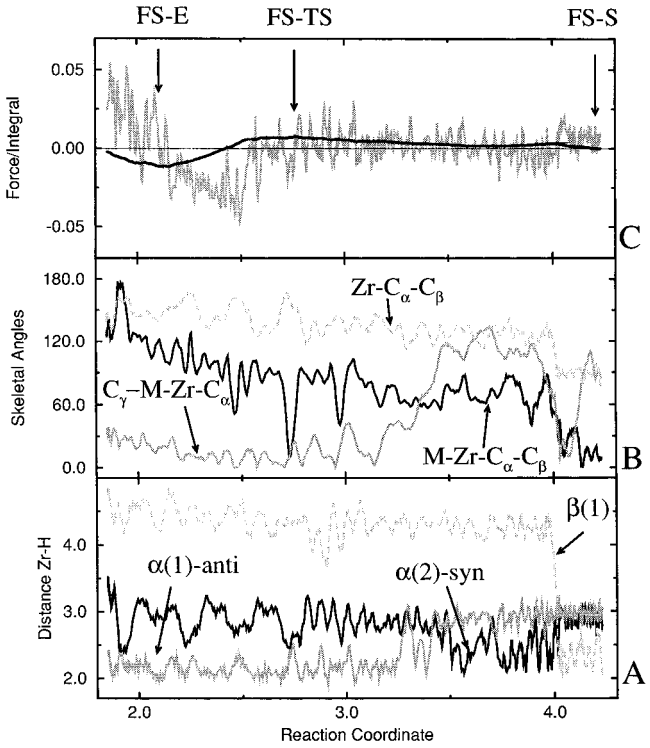

Figure 4. Structural and energetic quantities of the FS insertion simulation as a function of RCL. (A) Agostic bond distances between Zr and various hydrogen atoms. Only the three dominant agostic interactions are shown for the sake of clarity. (B) Skeletal angles of the $C_2H_4-Zr-C_2H_5$ moiety. (C) Force on the RC (shaded line) and its integral (full line). Arrows indicate the locations of the FS insertion precursor structure (FS-S), the FS insertion transition state (FS-TS), and the FS insertion γ-agostic product state (FS-E). Units as in Figure 2.

The force on the RC is predominantly positive in the beginning, as the β-agostic interaction is not yet destroyed and the ethyl and ethylene moieties interfere sterically, but drops to small negative values as soon as the ethyl group rotates out of the molecular midplane at 4.0 Å RCL. The force is only slightly positive until the transition state is reached, which is smeared out over 0.5 Å of RC (3−2.5 Å RCL). We locate the maximum of the integral curve (TS) at 2.76 Å RCL, in good agreement with a static ADF calculation which yields 2.769 Å.[3a] The γ-agostic product state is found at 2.15 Å RCL (ADF: 2.153 Å[3a]). Integrating the force on the constraint from the precursor to the TS and from the precursor to the product yields $\Delta F_N^{\ddagger} = +20$ kJ/mol and $\Delta F_N = -30$ kJ/mol, which is in good qualitative agreement with the values derived by Lohrenz et al.[3a] ($\Delta G^{\ddagger} = +8.55$ kJ/mol, $\Delta H = -34.2$ kJ/mol; Table 1). We estimate the error bars for ΔF_N values to be ±10 kJ/mol.

c. Simulation of the Back-Side (BS) Insertion. In order to obtain more detailed information about the back-side insertion than it was possible to extract from the FS-BS simulation, a CP-PAW simulation of the back-side insertion reaction **3b** has been done. The simulation was started from a back-side β-agostic conformation (Figure 5A). We used the M−C_α distance as a RC, scanning it from a value of 3.15 Å down to 1.85 Å, which forces the insertion of the ethylene into the Zr−C_α bond.

As already seen in Sections 3a and 3b, the β-agostic interaction stabilizing the precursor for back-side attack is much more stable than the β-agostic interaction of the front-side precursor. In the present simulation the β-agostic interaction (Figures 5A and 6A) is immobile until the reaction is quite finished, i.e. the δ-agostic product state is formed (Figures 5C and 6A), in which steric crowding of the alkyl chain around the Zr weakens the agostic bond and enables rotation of the terminal methyl to form a δ-agostic interaction via H(β_3). The relative immobility of the molecule during the reaction is confirmed by the structural quantities monitored in Figure 6B. Since the approaching ethylene molecule is not impeded by the steric bulk of the terminal methyl group, the $C_\gamma-M-Zr-C_\alpha$ torsion angle oscillates only ±40° around zero, slowly increasing from RC = 2.5 Å because the formation of a butyl chain conformation introduces a nonplanar structure. At the same time the $Zr-C_\alpha-C_\beta$ angle decreases, since the Zr−C_α bond is being broken. The $M-Zr-C_\alpha-C_\beta$ torsion angle, which serves to indicate out-of-plane rotation of the ethyl group, shows that no appreciable rotation takes place during the back-side insertion. Clear formation of an alkane chain occurs around 2.4 Å RCL (Figure 5C). The δ-agostic state was also found to be the direct product of back-side insertion by Lohrenz et al.[3a]

Since no evidence of potential energy minima adjacent to the back-side precursor has been detected, it can be assumed that the β-agostic precursor configuration as used in the present

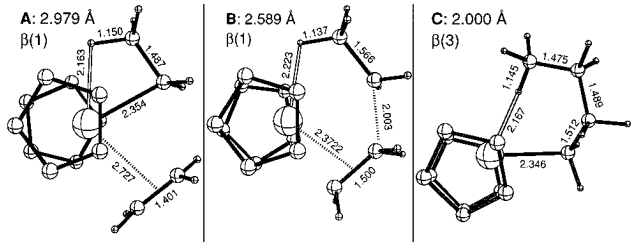

Figure 5. Selected snapshots from the BS reaction simulation, sequentially numbered from A to C. For legends and units see also Figure 1.

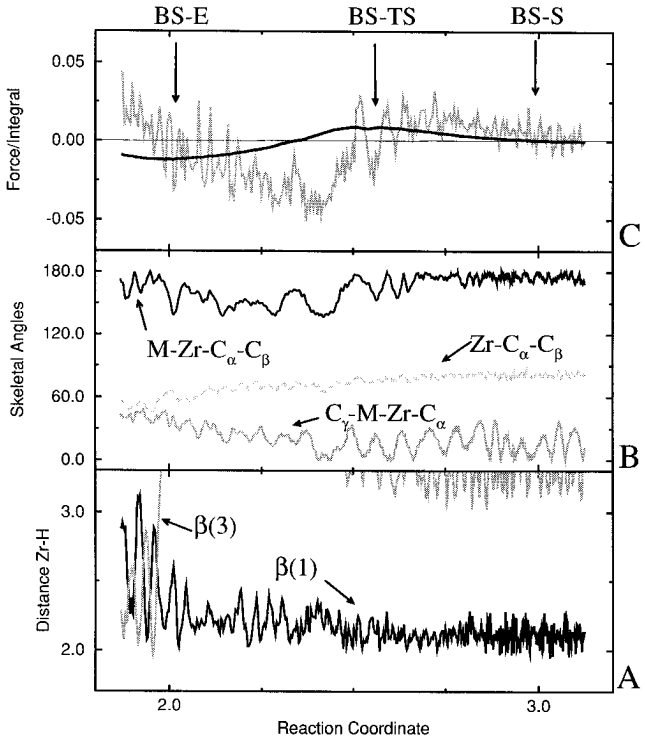

Figure 6. Structural and energetic quantities of the BS insertion simulation as a function of RCL. (A) Agostic bond distances between Zr and various hydrogen atoms. Only the two dominant agostic interactions are shown. (B) Skeletal angles of the $C_2H_4-Zr-C_2H_5$ moiety. (C) Force on the RC (shaded line) and its integral (full line). Arrows indicate the locations of the BS insertion precursor structure (BS-S), the BS insertion transition state (BS-TS), and the BS insertion δ-agostic product state (BS-E). Units as in Figure 2.

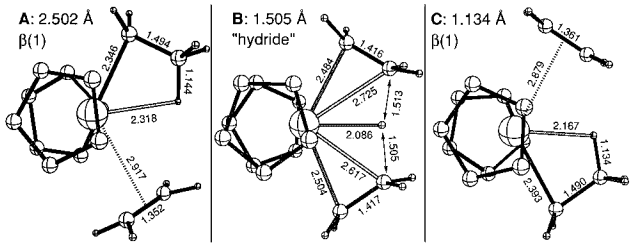

Figure 7. Selected snapshots from the hydrogen transfer reaction simulation, sequentially numbered from A to C. For legends and units see also Figure 1.

dynamics simulation is the true precursor for the BS insertion path.

Energetics. Integrating the force on the RC constraint yields $\Delta F_N^{\ddagger} = +21$ kJ/mol and $\Delta F_N = -28$ kJ/mol. As in the previous simulations, the locations of transition state and product on the RC agree perfectly with previous ADF calculations (Table 1). Similar to the front-side insertion path, the barrier is rather broad. We estimate the error bars for ΔF_N values to be ± 10 kJ/mol. In ref 3a, the insertion was calculated to have an electronic barrier of $\Delta H^{\ddagger}_{elec} = +28.4$ kJ/mol with a free energy of activation given by $\Delta G^{\ddagger} = +33.2$ kJ/mol at 300 K and an exothermicity of -24.9 kJ/mol, relative to the BS π-complex **1b** of Scheme 1.

d. Simulation of the Hydrogen Transfer (HT) Chain Termination. The polymer chain can be terminated by transfer of a hydride from a β-agostic hydrogen to the olefin, **4**. We studied the dynamics of this process by using the $C_\gamma-H(\beta_1)$ distance of Scheme 2 as a reaction coordinate, slowly decreasing it from a value of 2.5 Å down to 1.1 Å, which forces the elongation and subsequent rupture of the $C_\beta-H(\beta_1)$ bond and the formation of a $C_\gamma-H(\beta_1)$ bond. The starting geometry was similar to the one used in Section 3b.

Structure. Since the RC constraint effectively prohibits changes in the agostic bonding pattern, the initial β_1-agostic bond (Figure 7A) persists throughout the simulation (Figure 8A). All other hydrogen atoms can no longer partake in agostic bonding favored, so that at the transition state (RCL = 1.51 Å RCL, Figure 7B), the agostic bond is substantially strengthened which gives the TS geometry the semblance of a hydride, although the Zr−H distance is much longer than the typical Zr−hydride distance of 1.8 Å.

The plots of the $C_\beta-C_\alpha-Zr-M$ and the $C_\gamma-M-Zr-C_\alpha$ torsion angles (Figure 8B) show that the RC constraint largely prohibits out-of-plane motion of the ethyl and ethylene moieties. At the end of the reaction, the newly formed ethylene (previously ethyl) is no longer bound to the rest of the complex by a constraint. It dissociates from the complex at RCL = 1.15 Å. This dissociation is largely due to the abrupt release of energy from the rupture of the $C_\beta-H(\beta_1)$ bond.

Energetics. From Figure 8C it becomes obvious that the hydrogen transfer reaction has the most localized transition state of all the reactions investigated in this paper. Integrating the force on the constraint yields $\Delta F_N^{\ddagger} = +26$ kJ/mol (integrated from HT-S to HT-TS) and $\Delta F_N = -18$ kJ/mol (integrated from HT-S to HT-E). The integral from the product (HT-E) to the TS yields a $\Delta F^{\ddagger}$ of +44 kJ/mol. Since the reaction is per se thermoneutral ($\Delta F = 0$), our calculated ΔF value of -18 kJ/mol gives a direct estimate of the nonequilibrium character of the simulation. As expected for a short simulation, the error bars are of the same order of magnitude as the values themselves. From the average of both obtained $\Delta F^{\ddagger}$ values, we give a final $\Delta F_N^{\ddagger} = 35 \pm 15$ kJ/mol (ref 3a: $\Delta G^{\ddagger} = +29.6$ kJ/mol, Table 1). We find the transition state for the HT reaction at 1.51 Å RCL, in good agreement with ref 3a (Table 1).

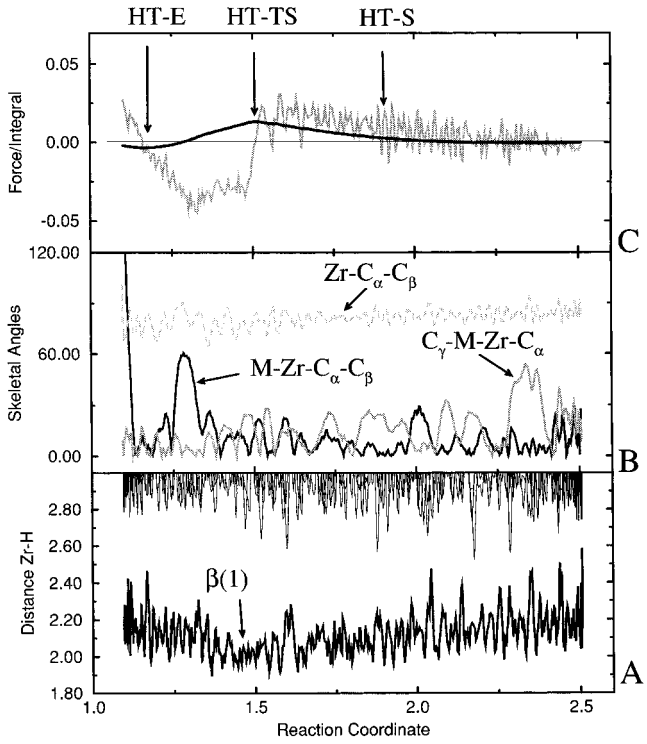

Figure 8. Structural and energetic quantities of the hydrogen transfer simulation as a function of RCL. (A) Agostic bond distances between Zr and various hydrogen atoms. The dominant agostic interaction is shown by a thick line, while all others are shown in the upper part of the graph as thin lines. (B) Skeletal angles of the $C_2H_4-Zr-C_2H_5$ moiety. (C) Force on the RC (shaded line) and its integral (full line). Arrows indicate the locations of the HT precursor structure (HT-S = FS-S), the HT transition state (HT-TS), and the HT product state (HT-E). Units as in Figure 2.

e. General Discussion. The activation barriers calculated by PAW for the FS ($\Delta F_N^{\ddagger} = +20$ kJ/mol) and BS ($\Delta F_N^{\ddagger} = +21$ kJ/mol) insertions are almost identical, whereas the HT activation has a higher barrier ($\Delta F_N^{\ddagger} = 35$ kJ/mol). However, Lohrenz et al.[3a] have pointed out that by taking into account vibrational quantum effects, FS and HT transition states become lowered in energy by 8.25 and 5.36 kJ/mol with respect to the β-agostic FS complex (FS-S = HT-S), whereas the BS transition state is stabilized by only 0.7 kJ/mol. Adding these quantum corrections (QC) taken from ref 3a to our PAW results gives a clear preference of the FS path over the other pathways (FS: $\Delta F_{N,QC}^{\ddagger} = +12$ kJ/mol; BS: $\Delta F_{N,QC}^{\ddagger} = +20$ kJ/mol; HT: $\Delta F_{N,QC}^{\ddagger} = +30$ kJ/mol). This effect of quantization does not appear in our classical treatment of the dynamics of the nuclei, but is certainly essential to consider.

In all simulations we found that the Cp rings do not change structurally during the reactions. They rotate almost freely, as has already been observed in a CP-PAW simulation of ferrocene.[25] The shape of the Cp−Zr−Cp skeleton does not change markedly during the reaction, and Cp−Cp tilt and Cp−Zr−Cp angles do not show any RC-dependent trends. Since the butyl product chain of the insertion processes studied has a comparatively huge configuration space, CPU time did not allow for enough time to pass in the FS and the BS simulation to observe the product rearrangement from γ- (FS) and δ- (BS) kinetic insertion products to the β-agostic resting state.

(25) Margl, P.; Schwarz, K.; Blöchl, P. E. *J. Chem. Phys.* **1994**, *100*, 8194.

4. Conclusion

Our molecular dynamics calculations allow the following conclusions to be drawn: (i) β-agostic resting states form the precursors for both back-side, front-side insertion and hydrogen transfer reaction, the latter two resting states being identical. The back-side β-agostic resting state is more stable than the front-side resting state, since the approaching olefin exerts steric pressure which destabilizes the front-side β-agostic interaction. (ii) The olefin in the precursor complexes is very mobile. It has been observed to dissociate from the metal center in room temperature simulations, which indicates that it probably partakes in rapid solvent exchange equilibria in solution. (iii) The ethylene can establish weak agostic interactions with the Zr center by simultaneous rotations about the C═C and Zr−M axes. These might be possible sources of C−H activation side reactions. (iv) The transition states determined for all three reactions are stabilized by strong agostic interactions. Agostic interactions have characteristic lifetimes between 0.5 and 2 ps for the front-side and back-side insertions, respectively. Agostic interactions flip on a time scale smaller than ≈0.1 ps. (v) The front-side insertion path is the most viable of all investigated reactions ($\Delta F_N^{\ddagger} = 20 \pm 10$ kJ/mol), followed by the back-side insertion path ($\Delta F_N^{\ddagger} = 21 \pm 10$ kJ/mol). The hydrogen transfer chain termination has a higher activation barrier than the former two reactions ($\Delta F_N^{\ddagger} = 35 \pm 15$ kJ/mol). We estimate that quantitative results can be achieved by increasing the simulation time by a factor of about 5. *A posteriori* addition of vibrational quantum corrections taken from ref 3a results in a strong preference of the FS path over the other pathways (FS: $\Delta F_{N,QC}^{\ddagger} = +12$ kJ/mol; BS: $\Delta F_{N,QC}^{\ddagger} = +20$ kJ/mol; HT: $\Delta F_{N,QC}^{\ddagger} = +30$ kJ/mol), which is in agreement with previous calculations.[3a] (vi) We tentatively identify the following stationary points encountered in our simulations: the β-agostic precursor complex for FS insertion (FS-S), which is identical to the precursor for the HT reaction (HT-S), and the β-agostic precursor complex for BS insertion (BS-S). These were assigned by the absence of other obvious stable configurations during the dynamics simulation. We locate one transition state for each reaction (FS-TS, BS-TS, and HT-TS). The transition state geometries are very similar to those found by Lohrenz et al.[3a] We find two (kinetic) products for FS and BS insertion, respectively, namely the γ-agostic FS product (FS-E) and the δ-agostic BS product (BS-E). Rearrangement of the butyl product chain is deemed feasible but was not observed due to insufficient simulation time.

Acknowledgment. This work has been supported by the National Sciences and Engineering Research Council of Canada (NSERC), as well as by the donors of the Petroleum Research Fund, administered by the American Chemical Society (ACS-PRF No 20723-AC3). P.M. would like to thank the Austrian Fonds zur Förderung der wissenschaftlichen Forschung (FWF) for financial support within project JO1099-CHE. J.C.W.L. thanks the Fonds der deutschen Chemie for a Liebig grant. The authors would like to thank T. K. Woo for interesting discussions.

JA953510F